Importance of the van Hove singularity in superconducting $PdTe_2$

Kyoo Kim,[1,2,*] Sooran Kim,[1,2,†] J. S. Kim,[2,3] Heejung Kim,[2] J.-H. Park,[1,2,4] and B. I. Min[2,‡]

[1]*Max Planck POSTECH/Hsinchu Center for Complex Phase Materials, Pohang University of Science and Technology, Pohang 37673, Korea*

[2]*Department of Physics, Pohang University of Science and Technology, Pohang 37673, Korea*

[3]*Center for Artificial Low Dimensional Electronic Systems, Institute for Basic Science, Pohang 37673, Korea*

[4]*Division of Advanced Materials Science, Pohang University of Science and Technology, Pohang 37673, Korea*

(Received 30 November 2017; revised manuscript received 19 March 2018; published 3 April 2018)

We have investigated the electronic, phononic, and superconducting properties of the transition-metal dichalcogenide superconductor $PdTe_2$, and explored the origin of different superconducting behaviors between $PdTe_2$ and its isostructural $PtTe_2$ that is nonsuperconducting. We have found that the saddle-point van Hove singularity (vHs) near the Fermi level, which interacts strongly with Te phonon modes, plays an important role in the BCS-type superconductivity of $PdTe_2$. We show that, with electron doping, the vHs in $PdTe_2$ shifts down toward the Fermi level to enhance T_c, as is consistent with the observed enhancement of T_c in Cu-doped $PdTe_2$. We ascribe the absence of superconductivity in $PtTe_2$ to the different dispersion behavior of the saddle-point vHs band from that of $PdTe_2$. We also suggest that this difference in the vHs band behaviors is responsible for the different structural responses of $PdTe_2$ and $PtTe_2$ to external pressure.

DOI: 10.1103/PhysRevB.97.165102

I. INTRODUCTION

Layered transition-metal dichalcogenide (TMD) systems have been studied extensively in many fields since the work of Wilson and Yoffe [1,2]. The two dimensionality of TMD material is of particular importance to bring about a variety of interesting physical properties, such as superconductivity, charge density wave (CDW), quantum criticality, and so on [3–5]. The simple structure of TMD, mainly composed of layers connected by a weak van der Waals interaction, makes the TMD a suitable platform for two-dimensional (2D) quantum materials. Namely, the TMD reveals the unique features of a 2D system, such as the simple structural variation by intercalation and possible exfoliation, which facilitates its fabrication for practical applications. In fact, a group of TMDs, such as MoS_2, WTe_2, and $MoTe_2$, has been intensively studied for spintronic materials, superconductors, and topological materials.

Recently, the topological surface state in $PdTe_2$ that is a CdI_2-type TMD was identified by using angle-resolved photoemission spectroscopy [6]. Furthermore, $PdTe_2$ and its isostructural materials [see Fig. 1(a)] were found to be type-II Dirac materials [7–11]. $PdTe_2$ exhibits superconductivity with $T_c \sim 1.78$ K [12], and so it is naturally anticipated that $PdTe_2$ would be a good candidate for a topological superconductor. Also, it was experimentally observed that Cu doping could enhance the T_c of $PdTe_2$ [13]. Intriguingly, its isostructural TMD, $PtTe_2$, is not a superconductor. The superconducting properties of $PdTe_2$, however, are rarely studied. It has been once proposed that a softened Γ phonon interacting with electrons in a tubelike Fermi surface (FS) is responsible for the superconductivity in $PdTe_2$ [14].

In this paper, we have investigated the electronic, phononic, and superconducting properties of $PdTe_2$, and compared its properties with those of $PtTe_2$ [9,14–24]. Using density functional theory (DFT) and density functional perturbation theory (DFPT), we have examined the electronic structures and the phonon dispersions, and electron-phonon interactions of $PdTe_2$ and $PtTe_2$. We have found that a dip structure in the phonon dispersion near Γ is important for the superconductivity, as Finlayson *et al.* [14] reported. However, we have identified that the electrons coupled with this mode are not the ones in the tubelike FS, as claimed by Finlayson *et al.* [14], but other ones in the band near the Fermi level (E_F) having the saddle-point van Hove singularity (vHs). The main difference in the electronic structures of $PdTe_2$ and $PtTe_2$ is found to be the behavior of this vHs band along the k_z direction, which indicates that the lack of superconductivity in $PtTe_2$ is related to the broad k_z dispersion of the vHs band. According to a pressure study by Soulard *et al.* [22], the structural response (structural rearrangement) to pressure was found to be abrupt for $PdTe_2$ but mild for $PtTe_2$. We suggest that this difference also comes from the different behaviors of the vHs band dispersions.

II. COMPUTATIONAL DETAILS

We have employed the full-potential linearized augmented plane-wave band method with local orbitals, implemented in WIEN2K for the band-structure calculations [25]. For the exchange-correlation potential, the Perdew-Burke-Ernzerhof (PBE) functional has been used. To take into account the relativistic effects of Pd (Pt) and Te, the spin-orbit interaction is included in a second variational manner with a large enough

*kyoo@mpk.or.kr

†Present address: John A. Paulson School of Engineering and Applied Sciences, Harvard University, Cambridge, MA 02138, USA.

‡bimin@postech.ac.kr

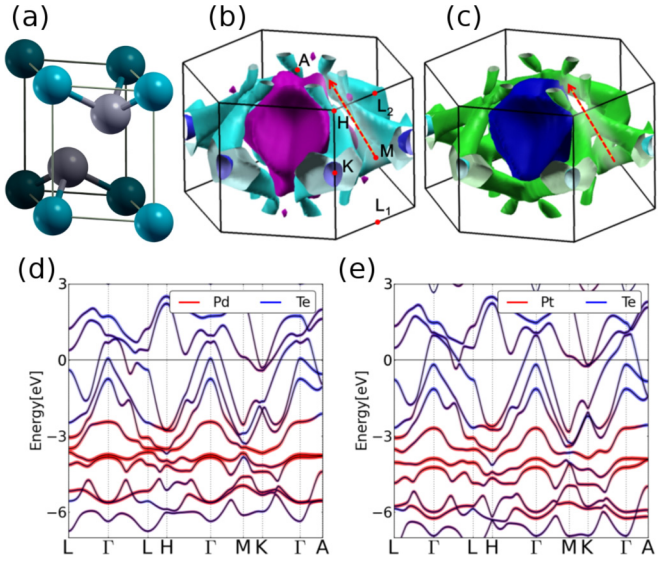

FIG. 1. (a) CdI_2-type structure of $PdTe_2$ and $PtTe_2$. Cyan-colored atoms denote Pd or Pt, while gray-colored atoms denote Te. (b) Fermi surface of $PdTe_2$. (c) Fermi surface of $PtTe_2$. Red dotted lines in (b) and (c) locate the position of saddle-point van Hove singularities in the BZ. (d) Band structure of $PdTe_2$, and (e) that of $PtTe_2$. Pd (Pt) and Te band components are represented by red and blue thick bands, respectively. Saddle points are seen near M just above E_F in the Pd (Pt)-Te hybridized band. Note that $PtTe_2$ has a larger bandwidth due to larger Pt-Te hybridization.

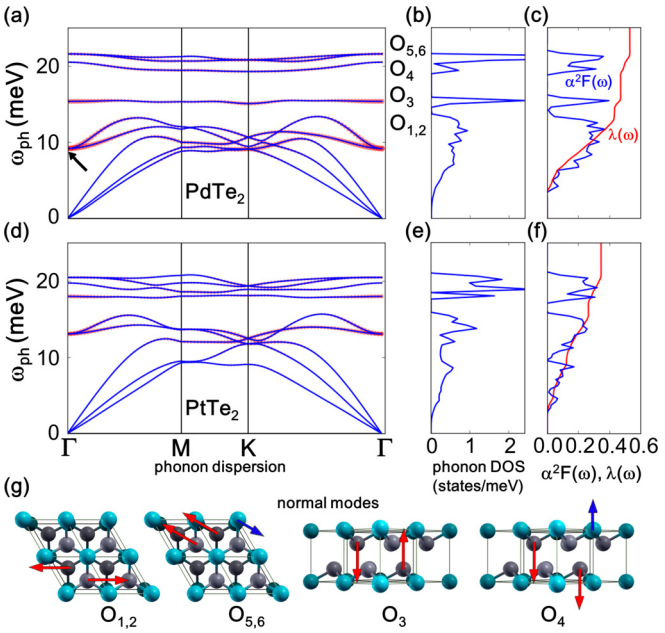

FIG. 2. (a) Phonon dispersion of $PdTe_2$. The size of the red circles is proportional to the phonon linewidth. Optical phonon modes are labeled as $O_{1,2}$, O_3, O_4, $O_{5,6}$. (b) Phonon density of states. (c) Eliashberg function $\alpha^2F(\omega)$ (blue) and $\lambda(\omega)$ (red) as a function of phonon frequency. (d)–(f) are corresponding figures for $PtTe_2$. (g) Normal modes of optical phonons $O_{1,2}$, O_3, O_4, $O_{5,6}$ at $q = \Gamma$. Red and blue arrows indicate Te and Pd displacements, respectively.

energy window up to 5 Ry and $19 \times 19 \times 13$ k points in the full Brillouin zone (FBZ) are used.

To study the phonon spectra and electron-phonon interaction, we have used the pseudopotential plane-wave band method implemented in QUANTUM ESPRESSO [26]. For phonon calculations, $5 \times 5 \times 5$ q points are used, and $10 \times 10 \times 10$ k points are used in the FBZ to get converged charge. For the calculation of the electron-phonon coupling constant λ, $40 \times 40 \times 40$ k points are used in the FBZ. We have fully relaxed the structure first using the VASP pseudopotential plane-wave package [27], and then the internal parameters of Te are optimized by using QUANTUM ESPRESSO prior to the calculation of the electron-phonon interaction. The spin-orbit interaction is considered for all calculations.

III. RESULTS AND DISCUSSIONS

A. Fermi surfaces and band dispersions

In Fig. 1, FSs and the band dispersion along the high-symmetry k points in the hexagonal Brillouin zone (BZ) for $PdTe_2$ and $PtTe_2$ are presented. Both compounds have six bands crossing E_F, which are grouped as three FS sheets with Kramers degeneracy: Γ-centered magenta- (blue-) colored FSs (hereafter B_1 FSs), K-centered cyan- (green-) colored FSs with tubelike branches (B_2), and small pockets near K in blue (cyan) color (B_3) for $PdTe_2$ ($PtTe_2$).

The topologies of FSs of two compounds are quite similar except for a few features. For $PdTe_2$, K-centered B_2 FSs are not connected, while for $PtTe_2$, the corresponding B_2 FSs are connected to each other [see the FSs along the red guidelines in Figs. 1(b) and 1(c)].

While this feature is not clearly seen in the band dispersions in Figs. 1(d) and 1(e), we will explain this feature more in Figs. 3 and 4 below. In the band dispersion, it is also seen that the bandwidth in $PtTe_2$ is larger than that in $PdTe_2$, despite the large lattice constant of $PtTe_2$, which is expected to originate from the more extended $5d$ band of Pt than the $4d$ band of Pd. Near E_F, the Te character is dominant except for the M-K path, where Pd(Pt)-Te hybridization is large.

B. Phonon spectra and electron-phonon coupling constants

We have calculated phonon spectra and electron-phonon coupling constants, utilizing the DFPT implemented in QUANTUM ESPRESSO [26]. Figures 2(a) and 2(b) show the phonon dispersion and phonon density of states (DOS) of $PdTe_2$. The size of the red circles on the dispersion curve represents the size of the phonon linewidth. As Finlayson *et al.* [14] pointed out, there is a dip structure, as indicated by an arrow in Fig. 2(a) near 15 meV at Γ in the lowest optical $O_{1,2}$ modes. Both $O_{1,2}$ and O_3 modes manifest large phonon linewidths, reflecting the strong electron-phonon interactions in these modes. As shown in Fig. 2(g), these normal modes are composed of Te displacements only, but they change the Te-Te interlayer distance as well as the Pd-Te intralayer distance.

Figure 2(c) shows the Eliashberg function $\alpha^2F(\omega)$ and the electron-phonon coupling constant $\lambda(\omega)$ as a function of

phonon frequency,

$$\alpha^2 F(\omega) = \frac{1}{2\pi N(\epsilon_F)} \sum_{q\eta} \frac{\lambda_{q\eta}}{\omega_{q\eta}} \delta(\omega - \omega_{q\eta}), \quad (1)$$

and $\lambda(\omega) = 2\int_0^\omega d\omega \frac{\alpha^2 F(\omega)}{\omega}$. Here, η denotes the phonon mode, and $\lambda_{q\eta}$,$\omega_{q\eta}$ are the electron-phonon coupling constant and phonon frequency for mode η at wave vector q, respectively. We estimated the superconducting T_c from the Allen-Dynes equation [28]

$$T_c = \frac{\omega_{\log}}{1.2} \exp\left(\frac{-1.04(1+\lambda)}{\lambda - \mu^*(1+0.62\lambda)}\right), \quad (2)$$

where $\omega_{\log}$ is the logarithmic averaged frequency, $\omega_{\log} = \exp(\frac{2}{\lambda}\int d\omega \log\omega \frac{\alpha^2 F(\omega)}{\omega})$.

Note that doubly degenerate phonon modes at Γ near 15 meV provide a large contribution to $\lambda(\omega)$, indicating their large contribution to superconductivity. These modes are the ones with the dip structure, pointed out by Finlayson *et al.* [14]. With the obtained $\lambda = 0.53$ in Fig. 2(c) and $\mu^* = 0.1$, T_c is estimated to be 1.79 K for $PdTe_2$, which is comparable to the experimental T_c of 1.78 K [12].

The overall features of the phonon dispersion and DOS for $PtTe_2$ in Figs. 2(d) and 2(e) are essentially the same as those of $PdTe_2$. But, compared to $PdTe_2$, the contribution of $O_{1,2}$ modes to $\lambda(\omega)$ is smaller for $PtTe_2$, and so $\lambda = 0.35$ is obtained, which is smaller than $\lambda = 0.53$ for $PdTe_2$ [see Fig. 2(f)]. The estimated T_c of $PtTe_2$ is 0.22 K, which is consistent with the fact that T_c of $PtTe_2$ is not observed down to $T = 1.2$ K.

Finlayson *et al.* [14] claimed that phonon modes with the dip structure are coupled with electrons in the tubelike FSs that span from K to near A in the hexagonal BZ. To identify which electronic bands are really coupled with these phonon modes, we have performed the DFT calculations for $PdTe_2$ with an imposed modulation corresponding to Te shear $O_{1,2}$ phonon modes. As shown in Fig. 3, due to modulations, there occur changes in the FSs near M toward A as well as the tubelike FSs. However, the change of the FSs near M is much more substantial, producing a Lifshitz-like transition in the topology of FS. According to the band dispersion in Fig. 1(d), there is a saddle-point vHs just above E_F near M. As the Pd-Te distance changes with modulations, the vHs band moves up or down across E_F, as shown in Figs. 3(c) and 3(d), which demonstrates the large electron-phonon coupling between the vHs band and $O_{1,2}$ phonon mode.

As we mentioned earlier, this modulation changes Pd-Te distances as well as the Te-Te distance. To check which structural character is more important, we have carried out similar calculations to those in Fig. 3 for the modulated monolayer systems $PdTe_2$ and $PtTe_2$. We get the same responses to normal modes for the monolayers, too, which implies that the intralayer Pd(Pt)-Te interaction is more important than the interlayer Te-Te interaction in tuning the energy positions of the saddle points. Note that the reduced Pd(Pt)-Te distance moves the vHs downward for both $PdTe_2$ and $PtTe_2$.

We mentioned in the Introduction that there exists a type-II Dirac point in $PdTe_2$, which might produce topological superconductivity. Note that the superconductivity in the above discussion arises mainly from the electrons at the vHs band near E_F, not from those at the type-II Dirac points that are

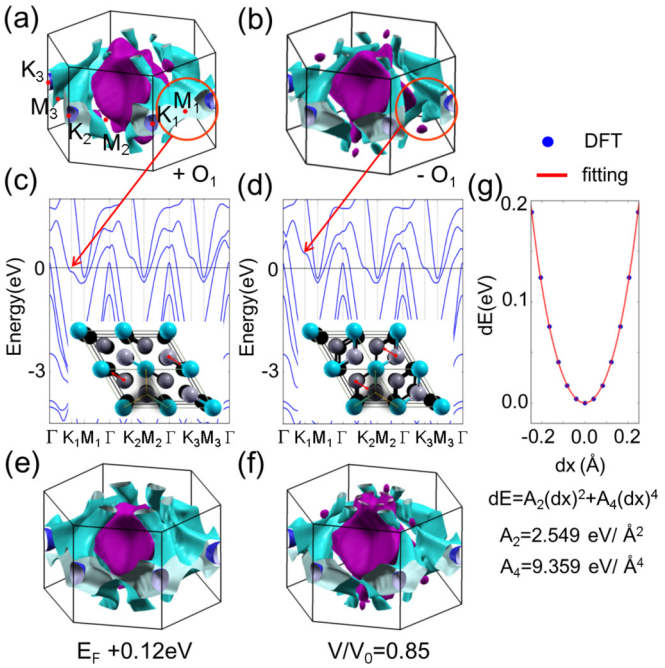

FIG. 3. (a) FS of $PdTe_2$ for the $+O_1$ modulated structure of the Te shear normal mode shown in the inset of (c), and (b) that for the $-O_1$ modulated structure shown in the inset of (d). Note that, in both cases, only Te atoms are displaced. (c), (d) Corresponding band structures to (a), (b). Green (yellow) dotted lines in the insets indicate short (long) Pd-Te bonds. Note that the main changes in the FSs occur near M_1, and that K-centered FSs are merged or separated with modulations. As the Pd-Te distance becomes short (long), the vHs at M shifts down (up). (e) FS of $PdTe_2$ for the electron-doped case with E_F shifted by 0.12 eV. (f) FS of $PdTe_2$ for the contracted volume by 15%. For both cases, K-centered FSs are merged together, reflecting that the vHs points fall down toward E_F. (g) The energy difference (dE) as a function of Te displacement (dx) from the equilibrium position for the Te shear normal mode O_1 (blue points). The red solid line is a fitted curve to the equation $dE = A_2 dx^2 + A_4 dx^4$. Note that there is a considerable anharmonic contribution.

located about 0.55 and 0.8 eV below E_F for $PdTe_2$ and $PtTe_2$, respectively [7–11]. This point has been explored recently by experiments, which manifest that the superconductivity in the type-II Dirac-semimetallic $PdTe_2$ is just a conventional one [12,29]. Nevertheless, the search for topological superconductivity in $PdTe_2$ and $PtTe_2$ will be quite interesting by tuning the binding energy of the Dirac points with external pressure or doping.

The strong electron-phonon coupling of the vHs electronic states shown in Figs. 2 and 3 suggests possible anharmonic responses to $O_{1,2}$ modes as in the case of MgB_2 [30]. To examine the possibility, we calculated the energy difference (dE) as a function of Te displacement (dx) from the equilibrium position for the O_1 normal mode in Fig. 3(g). The curve is fitted with a function of $dE = A_2 dx^2 + A_4 dx^4$. The harmonic coefficient A_2 and quadratic anharmonic coefficient A_4 are 2.549 eV/Å^2 and 9.359 eV/Å^4, respectively. Although the anharmonic term is not as large as that of MgB_2 [30], for which the whole boron p_σ band near E_F is strongly coupled with the E_{2g} phonon mode, the anharmonic contribution in $PdTe_2$ is not

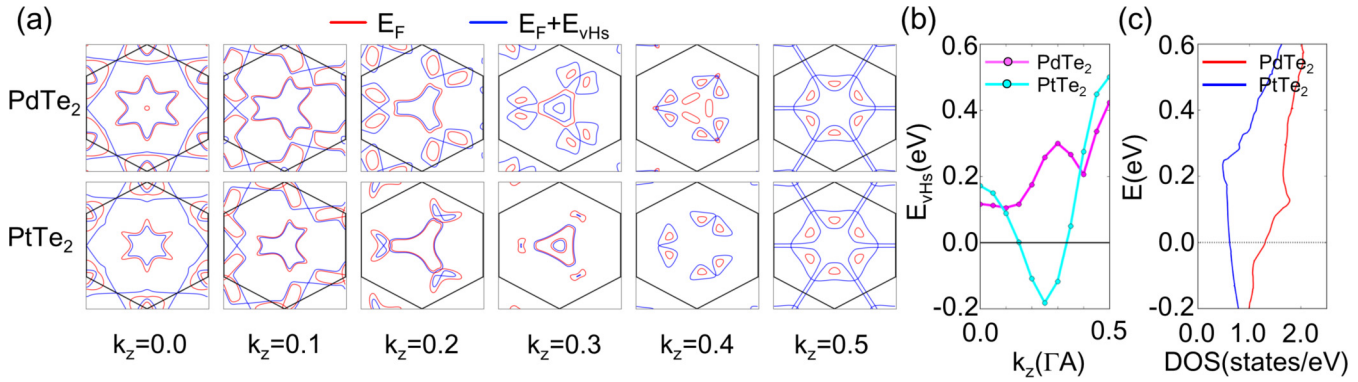

FIG. 4. (a) FSs for different k_z planes for $PdTe_2$ (upper row) and $PtTe_2$ (lower row), respectively. Red contours are FSs at E_F, while blue contours are FSs at the energy position of the vHs point E_{vHs}. (b) E_{vHs} positions of $PdTe_2$ and $PtTe_2$ for different k_z's. Note that E_{vHs} for $PdTe_2$ is less dispersive than that for $PtTe_2$. (c) Electron densities of states for $PdTe_2$ and $PtTe_2$ near the vHs points. Note that there is a pronounced peak structure only for $PdTe_2$.

negligible either. This anharmonic contribution originates from the electron-phonon interaction at the vHs points. However, for $PdTe_2$, the anharmonic contribution to the total energy is only about 1% of the harmonic contribution, so that the error from employing the standard Eliashberg theory for an anharmonic system $PdTe_2$ is expected to be minimal.

C. Dispersion behaviors of van Hove singularity (vHs) bands

As already shown in Figs. 1(d) and 1(e), the overall band structures of $PdTe_2$ and $PtTe_2$ are quite similar. But, there exists a sharp DOS peak at 0.12 eV above E_F for $PdTe_2$, while only a broad peak is observed for $PtTe_2$. The changes in the band structures with structural modulation corresponding to $O_{1,2}$ normal modes in both compounds show similar behaviors too along the high-symmetry k path (the $PtTe_2$ case is not shown).

With an electron doping of about 0.18 electrons per unit cell (corresponding to an E_F shift by 0.12 eV), the saddle points shift down toward E_F, and the M-centered FSs are connected, as presented in Fig. 3(e). Liu *et al.* [13] reported the enhancement of T_c in Cu-intercalated $PdTe_2$ that corresponds to electron-doped $PdTe_2$. By the Cu intercalation, the estimated E_F shift was merely ~16 meV, but there occurred a change in the lattice parameters. Hence we have performed the DFT calculations for $PdTe_2$ with 15% volume contraction. Then, the M-centered FSs start to merge together, as shown in Fig. 3(f). This feature suggests that the vHs band closer to E_F produces a more enhanced T_c, unless another structural transition relieves the vHs.

To explore why superconductivity does not appear in $PtTe_2$, we have examined more carefully the near-E_F band structures and B_2 FS topologies of both compounds. Figure 4 presents the FS cuts for different k_z's for both compounds. The contours in red represent B_2 FSs at E_F, and blue contours represent isosurfaces of the B_2 band at $E_F + E_{vHs}$, where E_{vHs} is the energy position of the saddle-point vHs with respect to E_F. The amount of E_{vHs} for each k_z is plotted in Fig. 4(b). It is noteworthy that, in $PdTe_2$, the energy positions of the saddle points are less dispersive compared to those in $PtTe_2$, which is indeed the reason for a sharper DOS peak in $PdTe_2$, as shown in Fig. 4(c). We deduce that these different behaviors of near-E_F vHs points are responsible for the presence and absence of superconductivity in $PdTe_2$ and $PtTe_2$, respectively [31,32].

In a recent work by Cheng *et al.* [33], the doping dependence of the superconducting temperature for an isostructural material $PtSe_2$ was studied [33]. The theoretical T_c of $PtSe_2$ was estimated to be 0.002 K. With an electron doping of $0.5e^-$ per formula unit cell, T_c increases up to 2.15 K. They claimed that the mechanism of the superconductivity in doped $PtSe_2$ is related to the softening of acoustic phonon modes. We noticed that the vHs at the K point is about 0.5 eV above E_F for pristine $PtSe_2$. However, with doping, the vHs point becomes close to E_F, and the band dispersion becomes similar to that of $PdTe_2$. Therefore, there is still a possibility that the contribution of $O_{1,2}$ optical phonon modes to superconductivity is as important as that of the softened acoustic phonon modes. Actually, in Fig. S4(d) of Ref. [33], the contribution of phonons with $\omega \sim 100$–$150\ cm^{-1}$, where $O_{1,2}$ modes reside, to λ is seen to be considerable. Further study is needed on this aspect.

D. Structural responses to pressure

Soulard *et al.* [22] showed that, under pressure, the structural parameters change abruptly at around 20 GPa, which corresponds to a 10% volume contraction in $PdTe_2$, while in $PtTe_2$, the changes are mild up to 30 GPa. They claimed that this difference comes from the difference in the hybridization between Pd-Te and Pt-Te. According to our calculation, when we contract the volume of $PdTe_2$ by 15%, all the saddle points shift down to E_F and the M-centered FSs start to merge together [see Fig. 3(f)]. We suspect that the instability by the saddle-point vHs near E_F might be a driving force for such an abrupt change in the lattice parameters of $PdTe_2$. However, for $PtTe_2$, the saddle points cross E_F rather gradually with pressure, and so the change in lattice parameters also becomes mild. Even when the spin-orbit interaction of $PtTe_2$ is turned off, the energy positions of the saddle points do not change, indicating that the structure of the vHs points is correlated more to the size of Pt/Pd than to the spin-orbit interaction.

IV. CONCLUSION

Employing the DFT and DFPT, we have studied the electronic and phonon band structures, and the superconducting and structural properties of the layered TMDs, $PdTe_2$ and

$PtTe_2$. Our study reveals that the saddle-point vHs near E_F plays essential roles in both the BCS-type superconductivity of $PdTe_2$ and the abrupt change in the lattice parameters under pressure. We suggest that the absence of superconductivity and also the mild change in the lattice parameters under pressure in isostructural $PtTe_2$ are due to the different dispersion behavior of the near-E_F saddle-point vHs band from that in $PdTe_2$.

ACKNOWLEDGMENTS

We appreciate K.-T. Ko for fruitful discussions. This work was supported by the NRF Grant (Contracts No. 2016R1D1A1B02008461, No. 2017M2A2A6A01071297, No. 2017R1A2B4005175, and No. 2011-0030785), Max-Plank POSTECH/KOREA Research Initiative (Grant No. 2016K1A4A4A01922028), and KISTI (Project No. KSC-2016-C3-0062).

[1] J. A. Wilson and A. D. Yoffe, Adv. Phys. **18**, 193 (1969).
[2] J. A. Wilson, F. J. Di Salvo, and S. Mahajan, Adv. Phys. **24**, 117 (1975).
[3] K. Rossnagel, J. Phys.: Condens. Matter **23**, 213001 (2011).
[4] M. Calandra and F. Mauri, Phys. Rev. Lett. **106**, 196406 (2011).
[5] K. E. Wagner, E. Morosan, Y. S. Hor, J. Tao, Y. Zhu, T. Sanders, T. M. McQueen, H. W. Zandbergen, A. J. Williams, D. V. West, and R. J. Cava, Phys. Rev. B **78**, 104520 (2008).
[6] Y. Liu, J. Zhao, L. Yu, C. Lin, A. Liang, C. Hu, Y. Ding, S. He, L. Zhao, G. Liu, X. Dong, J. Zhang, C. Chen, Z. Xu, H. Weng, X. Dai, Z. Fang, and X. Zhou, Chin. Phys. Lett. **32**, 067303 (2015).
[7] H.-J. Noh, J. Jeong, E.-J. Cho, Kyoo Kim, B. I. Min, and B.-G. Park, Phys. Rev. Lett. **119**, 016401 (2017).
[8] M. Yan, H. Huang, K. Zhang, E. Wang, W. Yao, K. Deng, G. Wan, H. Zhang, M. Arita, H. Yang, Z. Sun, H. Yao, Y. Wu, S. Fan, W. Duan, and S. Zhou, Nat. Commun. **8**, 257 (2017).
[9] F. Fei, X. Bo, R. Wang, B. Wu, J. Jiang, D. Fu, M. Gao, H. Zheng, Y. Chen, X. Wang, H. Bu, F. Song, X. Wan, B. Wang, and G. Wang, Phys. Rev. B **96**, 041201(R) (2017).
[10] R. C. Xiao, P. L. Gong, Q. S. Wu, W. J. Lu, M. J. Wei, J. Y. Li, H. Y. Lv, X. Luo, P. Tong, X. B. Zhu, and Y. P. Sun, Phys. Rev. B **96**, 075101 (2017).
[11] K. Zhang, M. Yan, H. Zhang, H. Huang, M. Arita, Z. Sun, W. Duan, Y. Wu, and S. Zhou, Phys. Rev. B **96**, 125102 (2017).
[12] S. Das, Amit, A. Sirohi, L. Yadav, S. Gayen, Y. Singh, and G. Sheet, Phys. Rev. B **97**, 014523 (2018).
[13] Y. Liu, J. Zhao, L. Yu, C. Lin, C. Hu, D. Liu, Y. Peng, Z. Xie, J. He, and C. Chen, Chin. Phys. B **24**, 067401 (2015).
[14] T. R. Finlayson, W. Reichardt, and H. G. Smith, Phys. Rev. B **33**, 2473 (1986).
[15] G. W. Ryan and W. L. Sheils, Phys. Rev. B **61**, 8526 (2000).
[16] H. W. Myron, Solid State Commun. **15**, 395 (1974).
[17] A. E. Dunsworth, J. Low Temp. Phys. **19**, 112 (1975).
[18] J.-P. Jan and H. L. Skriver, J. Phys. F: Met. Phys. **7**, 1719 (1977).
[19] P. J. Orders, J. Liesegang, R. C. G. Leckey, J. G. Jenkin, and J. D. Riley, J. Phys. F: Met. Phys. **12**, 2737 (1982).
[20] G. Y. Guo and W. Y. Liang, J. Phys. C **19**, 995 (1986).
[21] S. Jobic, R. Brec, and J. Rouxel, J. Solid State Chem. **96**, 169 (1992).
[22] C. Soulard, P. E. Petit, P. Deniard, M. E. Evain, S. Jobic, M.-H. Whangbo, and A.-C. Dhaussy, J. Solid State Chem. **178**, 2008 (2005).
[23] J. Guggenheim, F. Hulliger, and J. Müller, Helv. Phys. Acta **34**, 408 (1961).
[24] H. Leng, C. Paulsen, Y. K. Huang, and A. de Visser, Phys. Rev. B **96**, 220506(R) (2017).
[25] P. Blaha, K. Schwarz, G. K. H. Madsen, D. Kvasnicka, and J. Luitz, *WIEN2k, An Augmented Plane Wave + Local Orbitals Program for Calculating Crystal Properties* (Karlheinz Schwarz, Techn. Universitat Wien, Austria, 2001).
[26] P. Giannozzi, S. Baroni, N. Bonini, M. Calandra, R. Car, C. Cavazzoni, D. Ceresoli, G. L. Chiarotti, M. Cococcioni, I. Dabo, A. Dal Corso, S. Fabris, G. Fratesi, S. de Gironcoli, R. Gebauer, U. Gerstmann, C. Gougoussis, A. Kokalj, M. Lazzeri, L. Martin-Samos *et al.*, J. Phys.: Condens. Matter **21**, 395502 (2009).
[27] G. Kresse and J. Furthmüller, Phys. Rev. B **54**, 11169 (1996); Comput. Mater. Sci. **6**, 15 (1996).
[28] P. B. Allen and R. C. Dynes, Phys. Rev. B **12**, 905 (1975).
[29] Amit and Y. Singh, Phys. Rev. B **97**, 054515 (2018).
[30] T. Yildirim, O. Gülseren, J. W. Lynn, C. M. Brown, T. J. Udovic, Q. Huang, N. Rogado, K. A. Regan, M. A. Hayward, J. S. Slusky, T. He, M. K. Haas, P. Khalifah, K. Inumaru, and R. J. Cava, Phys. Rev. Lett. **87**, 037001 (2001).
[31] W. Sano, T. Koretsune, T. Tadano, R. Akashi, and R. Arita, Phys. Rev. B **93**, 094525 (2016).
[32] E. Cappelluti and L. Pietronero, Phys. Rev. B **53**, 932 (1996).
[33] C. Cheng, J.-T. Sun, M. Liu, X.-R. Chen, and S. Meng, Phys. Rev. Mater. **1**, 074804 (2017).